generally the same behavior can be observed as for the higher Reynolds number case, so that the same remarks apply.[6]

Boundary-Layer Flow

The boundary-layer flow was calculated with an elliptic finite-volume procedure[14] using 122 nonuniformly spaced grid points across the layer (for further details see Ref. 6). The calculation domain covered a streamwise distance x such that $Re_\theta = 300$ at the inflow and $Re_\theta = 1410$ at the outflow boundary. Table 2 compares for the two x positions, where the momentum-thickness Reynolds number Re_θ is 670 and 1410, the friction coefficient c_f and shape parameter H predicted by the various models with the DNS data. At both Reynolds numbers, the new model gives the best overall agreement. In particular, the c_f value predicted by the RMM model is considerably closer to the data than c_f predicted by any other model. For the profiles of U, $\overline{uv}$, k, and ϵ, basically the same behavior can be observed as for the channel flow. The LS model predicts too high a velocity in the outer region of the boundary layer, but for this flow the MS model results are also slightly too high (in the intermediate region), whereas the LB and RMM models yield very good agreement with the DNS profile.[6] Very near the wall, the $\overline{uv}$ distribution is again predicted best by the RMM model, a result that explains the superior prediction of the c_f values. But near the boundary-layer edge, all models except the LB model yield too fast an approach of the shear stress to zero.[6] Concerning the k distribution (Fig. 2a), the new model is again the most accurate one near the wall. But also in the boundary-layer case it predicts a somewhat excessive k peak, whereas the LB and MS models reproduce the peak value correctly. At the boundary-layer edge, the LB model predicts the approach of k to zero correctly, whereas all of the other models predict too fast an approach. The ϵ distribution resulting from the RMM model (Fig. 2b) is very close to the one for the channel flow shown in Fig. 1a. On the other hand, the DNS data show somewhat larger ϵ values very near the wall for the boundary layer than for the channel flow, and hence the agreement is not as good as in the channel flow case. However, the ϵ prediction by the RMM model is still by far the best. Virtually the same remarks can be made on the calculations of the $Re_\theta = 670$ boundary layer.[6]

All of the results have been checked for grid independence by performing calculations on different grids. It was found that grid independence in the critical near-wall region requires the first grid point to be placed at $y^+ = 0.5 - 1$. Use of fewer than 61 grid points in the normal direction with fewer than 20 points in the region $0 < y^+ < 100$ led to a rapid deterioration of the results. In particular, ϵ_w was found to be sensitive to the number of grid points placed within the buffer layer.

IV. Conclusions

The low Re k-ϵ model proposed by Rodi and Mansour[2] on the basis of DNS data was complemented by a damping function multiplying the destruction term in the model ϵ equation. First a function involving $\tilde{\epsilon}$ as defined by Hanjalic and Launder[7] was tried. Very near the wall, this method led to an underprediction of ϵ and to an unrealistic ϵ balance. A different definition of $\tilde{\epsilon}$ was therefore introduced, and some of the constants in the RM model were retuned. The resulting modified version (RMM) yielded generally good predictions of all major quantities in developed channel and boundary-layer flows compared with the DNS data. The model mimics correctly the change in sign of the near-wall production P_ϵ^3, which in turn is mainly responsible for the fairly realistic simulation of the ϵ distribution near the wall. However, the model produces some excessive up-down behavior of ϵ in this region and requires further fine tuning of the constants. Also, the model has to be tested in the future for other flow situations.

References

[1]Patel, V. C., Rodi, W., and Scheuerer, G., "Turbulence Models for Near-Wall and Low-Reynolds Number Flows: A Review," *AIAA Journal,* Vol. 23, 1985, pp. 1308–1319.

[2]Rodi, W., and Mansour, N. N., "Low-Reynolds Number k-ϵ Modeling with the Aid of Dirct Simulation Data," *Journal of Fluid Mechanics,* Vol. 250, 1993, pp. 509–529.

[3]Kim, J., Moin, P., and Moser, R., "Turbulence Statistics in Fully Developed Channel Flow at Low Reynolds Number," *Journal of Fluid Mechanics,* Vol. 177, 1987, pp. 133–166.

[4]Kim, J., private communication, NASA Ames Research Center, 1990.

[5]Spalart, P. R., "Direct Simulation of a Turbulent Boundary Layer up to $R_\theta = 1410$," *Journal of Fluid Mechanics,* Vol. 187, 1988, pp. 61–98.

[6]Michelassi, V., Rodi, W., and Zhu, J., "Testing a Low Reynods Number k-ϵ Turbulence Model Based on Direct Simulation Data," Univ. of Karlsruhe, Rept. SFB 210/T/83, Karlsruhe, Germany, Dec. 1992.

[7]Hanjalic, K., and Launder, B. E., "Contribution Towards a Reynolds-Stress Closure for Low-Reynolds Number Turbulence," *Journal of Fluid Mechanics,* Vol. 74, 1976, pp. 593–610.

[8]Launder, B. E., and Sharma, B. I., "Application of the Energy-dissipation Model of Turbulence to the Calculation of Flow near a Spinning Disc," *Letters in Heat and Mass Transfer,* Vol. 1, 1974, pp. 131–138.

[9]Lam, C. K. G., and Bremhorst, K. A., "Modified Form of the k-ϵ Model for Predicting Wall Turbulence," *Journal of Fluids Engineering,* Vol. 103, 1981, pp. 456–460.

[10]Michelassi, V., and Shih, T. H., "Low Reynolds Number Two-Equation Modelling of Turbulent Flows," NASA TM-104368, May 1991.

[11]So, R. M. C., Zhang, H. S., and Speziale, C. G., "Near-Wall Modeling of the Dissipation Rate Equation," *AIAA Journal,* Vol. 29, 1991, pp. 2069–2076.

[12]Coleman, G. N., and Mansour, N. N., "Simulation and Modeling of Homogeneous Compressible Turbulence Under Isotropic Mean Compression," *Proceedings of the 8th Turbulent Shear Flows Symposium,* Munich, Germany, Sept. 9–11, 1991, pp. 21-3-1–21-3-6.

[13]Michelassi, V., "Testing of Turbulence Models by an Artifical Compressibility Solution Method," Univ. of Karlsruhe, Rept. SFB 210/T/49, Karlsruhe, Germany, 1988.

[14]Rodi, W., Majumdar, S., and Schönung, B., "Finite-Volume Methods for Two-Dimensional Incompressible Flows with Complex Boundaries," *Computational Methods in Applied Mechanics and Engineering,* Vol. 75, 1989, pp. 369–392.

Evaluation of Baldwin-Barth Turbulence Model with an Axisymmetric Afterbody-Exhaust Jet Flowfield

M. Kandula*
Lockheed Engineering and Sciences Company, Houston, Texas 77058
and
P. G. Buning†
NASA Ames Research Center, Moffett Field, California 94035

Nomenclature

c_p	= pressure coefficient
D_{max}	= maximum body diameter
k	= turbulent kinetic energy
M	= Mach number

Received Nov. 6, 1992; presented as Paper 93-0418 at the AIAA 31st Aerospace Sciences Meeting, Reno, NV, Jan. 11–14, 1993; revision received March 1, 1993; accepted for publication March 2, 1993.

*Group Leader, Computational Fluid Dynamics. Senior Member AIAA.
†Research Scientist. Senior Member AIAA.

p	= static pressure
p_0	= pitot pressure
Pr	= Prandtl number
Re	= Reynolds number, $u_\infty D_{max}/\nu_\infty$
Re_t	= turbulence Reynolds number, $k^2/(\nu\varepsilon)$
T	= temperature
u^*	= friction velocity, $\sqrt{\tau_w/\rho_w}$
u, v, w	= Cartesian velocity components
x, y, z	= Cartesian coordinate directions
x', y', z'	= x/D_{max}, y/D_{max}, z/D_{max}
z^+	= dimensionless wall coordinate, zu^*/ν
γ	= specific heat ratio
$\Delta x, \Delta z$	= local grid spacings in x and z directions
ϵ	= rate of dissipation of k
μ	= dynamic viscosity
ν	= kinematic viscosity
ρ	= density
τ_w	= wall shear stress

Subscripts

j	= jet
t	= total (stagnation)
w	= wall
∞	= freestream

Superscript

$'$	= dimensionless quantities

Introduction

SEPARATED flow over an afterbody with a propulsive jet contributes significantly to the total drag of space launch vehicles, aircraft, and missiles. The high-pressure jet issuing from the nozzle interacts with the afterbody flow through an inviscid plume effect and a turbulent mixing process in the shear layers, and causes upstream influence on the afterbody flow. The accuracy with which the separated flow and the jet mixing layer growth are predicted is dependent on the accuracy of the turbulence model considered in the analysis.

Previous solutions for a circular arc afterbody/exhaust jet configuration[1,2] by Deiwert et al.[3] using the Baldwin-Lomax algebraic model,[4] and by Peace[5] using both the Baldwin-Lomax model and a two-equation k-ϵ model of Chien[6] show that the surface pressure in the separated region is grossly overpredicted. Solutions by Peace[5] for jet mixing layer growth show underprediction of data. Thus it appears that turbulence modeling needs further investigation for the simulation of separated flows and mixing layers. The primary objective of this work is to validate the recently developed Baldwin-Barth one-equation turbulence model[7] to describe the preceding type of flows. This model, which solves for Re_t, is derived from a standard k-ϵ model with the assumption of equality of production and dissipation rate of turbulence, and with damping functions for the wall region. The transition from the wall-bounded region to the wake is made by simply turning off the viscous damping functions in the wake region.

The Baldwin-Barth one-equation turbulence model has been implemented in various three-dimensional central-difference and upwind finite volume compressible and/or incompressible Navier-Stokes codes (ARC3D, CFL3D, INS3D, USA). However, studies on validation of this turbulence model are relatively few. To the authors' knowledge, the Baldwin-Barth model has not been tested for the type of separated and shear flows characteristic of the afterbody/jet exhaust system under consideration, and this forms an important contribution of the present report based on Ref. 8.

Analysis

The compressible thin-layer Navier-Stokes code, Overflow, described in Ref. 9, solves the three-dimensional, unsteady flow governing equations in conservative form in generalized coordinates (ξ, η, ζ) that are transformations of the rectangular Cartesian space (x, y, z).

Computational Grid

The maximum body diameter D_{max} of 15.4 cm is taken as the reference length in the calculations. The afterbody length is $0.8D_{max}$, and the jet diameter is $0.5D_{max}$. Figure 1 shows the computational grid. Two separate grids are used for the body and the jet, with one grid point overlap. A 70×70 grid (streamwise $\times$ radial) is considered for the body, and a 90×119 grid is employed for the jet grid. The value of z^+ for the first grid points from the wall of the afterbody ranges from 0.3 to 3 along the wall, with the grid cell thickness $\Delta z'$ of about 0.00002. The clustering for the jet grid is such that the grid cell thickness $\Delta z'$ is 0.005 near the jet axis and 0.00002 near the nozzle wall where the jet shear layer develops.

Boundary Conditions

No-slip and adiabatic wall conditions are applied at the solid body. The pressure at the wall is obtained from zero normal pressure gradient on the body surface. At the inflow a velocity distribution is specified with an estimated boundary-layer thickness of $\delta'=0.0525$. At the top (free) boundary, the freestream variables are specified. At the nozzle exit, a viscous boundary layer is included with an estimated thickness δ' of 0.01. To accelerate the solution, the nozzle exit conditions are extended to the outflow for the initial condition. The outflow variables are obtained from the interior solution by linear extrapolation. All boundary conditions are applied explicitly.

Results and Discussion

All the computations are carried out for steady-state conditions with $M_\infty=0.8$, and $M_j=1.0$. The value of p_j/p_∞ is 1.532, and the jet pressure ratio p_{tj}/p_∞ is 2.9. The total temperature ratio for the nozzle $T_{tj}/T_{t\infty}=1$. Values of $Pr=0.7$ and $\gamma=1.4$ are assumed. Local time stepping is employed to accelerate solution convergence, which is achieved in about 4000 iterations. The reverse flow region extends from the tail end of the afterbody to some distance downstream of the nozzle exit plane.[8]

Afterbody Pressure

A comparison of the afterbody pressures with the experimental data is presented in Fig. 2. The data show that the boundary layer separates at about $x'=-0.29$, giving rise to a pressure plateau. The

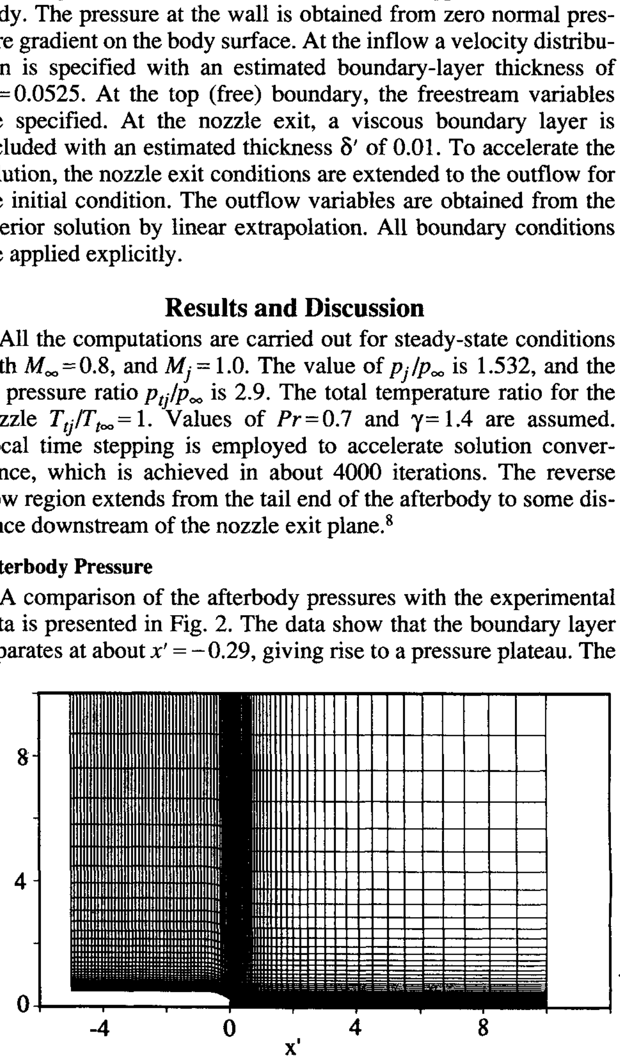

Fig. 1 Computational grid.

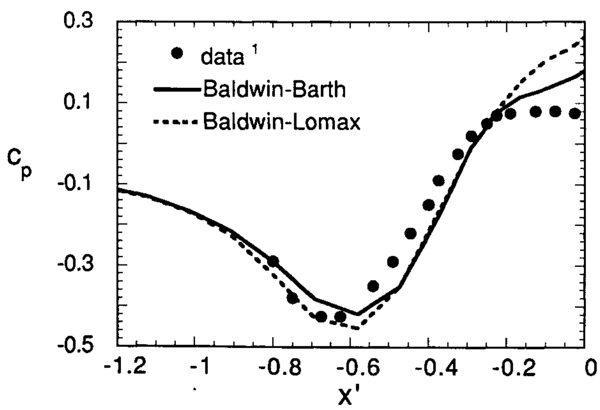

Fig. 2 Afterbody surface pressure comparison.

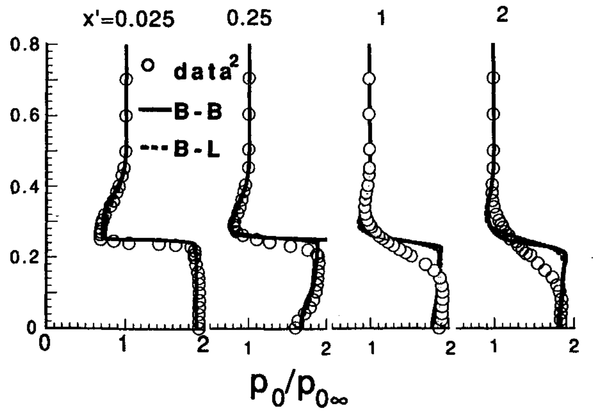

Fig. 3 Comparison of jet radial pitot pressure.

predicted locations of separation are $x' = -0.298$ and -0.251 for the Baldwin-Barth and Baldwin-Lomax models, respectively. In the attached region, both Baldwin-Barth and Baldwin-Lomax models agree well with the data. In the separated region, the Baldwin-Barth model compares considerably better with the data, as compared to the Baldwin-Lomax model. However, there still appears to be some overprediction of c_p by the Baldwin-Barth model and, hence, the underprediction of the drag.

Mixing Layer Predictions

The mixing layer predictions are compared in Fig. 3a–3d with the pitot pressure data at various streamwise stations in the jet ($x' = 0.025$, 0.25, 1.0, and 2.0). In general the predictions from the Baldwin-Barth model are close to those from the Baldwin-Lomax model in describing mixing layers. Both turbulence models clearly underestimate the mixing and, hence, entrainment of fluid from the external flow region. The deviations of the models with the data is seen to increase with increasing x'.

The Baldwin-Barth model, being built upon the k-ϵ model, should be expected to predict too small a wake growth, since the k-ϵ model is known to underpredict the far-wake growth. The assumption of equality of turbulence production and dissipation rates (equilibrium turbulence) over the entire shear layer/mixing layer is also not realistic. The flow under consideration undergoes abrupt changes in the turbulence structure, i.e., from a boundary-layer flow to a free shear flow with quite different length scales.

Conclusion

The present study of an afterbody/exhaust jet flowfield has shown that the Baldwin-Barth one-equation turbulence model offers a definitive improvement in the prediction of surface pressure in the pressure-gradient induced separation region over the Baldwin-Lomax algebraic model. However, there still is some overprediction of the data by the one-equation model. In the mixing layer, the Baldwin-Barth model considerably underpredicts the growth of the mixing layer, as does the Baldwin-Lomax model. The Baldwin-Barth model needs improvement for the prediction of pressure-gradient induced separation and mixing layer growth. Higher order turbulence models including multiscale models should be investigated for an accurate description of separated flows and mixing layer growth.

Acknowledgment

This work was supported by the Aerosciences Branch of NASA Johnson Space Center under Contract NAS 9-17900, with F. W. Martin Jr. as Technical Monitor.

References

[1]Reubush, D. E., and Runckel, J., "Effect of Fineness Ratio on Boattail Drag on Circular-Arc Boattail Afterbodies Having Closure Ratios of 0.50 with Jet Exhaust Mach Numbers Up to 1.3," NASA TN D-7192, May 1973.

[2]Mason, N. L., and Putnam, L. E., "Pitot Pressure Measurements in Flow Fields Behind Circular-Arc Nozzles with Exhaust Jets at Subsonic Freestream Mach Numbers," NASA TM 80169, 1979.

[3]Deiwert, G. S., Andrews, A. E., and Nakahashi, K., "Theoretical Analysis of Aircraft Afterbody Flows," *Journal of Spacecraft and Rockets*, Vol. 24, No. 6, 1987, pp. 496–503.

[4]Baldwin, B. S., and Lomax, H., "Thin-Layer Approximation and Algebraic Model for Separated Turbulent Flows," AIAA Paper 78-257, Jan. 1978.

[5]Peace, A. J., "Turbulent Flow Predictions for Afterbody Nozzle Geometries Including Base Effects," *Journal of Propulsion and Power*, Vol. 7, No. 3, 1991, pp. 396–403.

[6]Chien, K. Y., "Predictions of Channel and Boundary Layer Flows with a Low-Reynolds-Number Turbulence Model," *AIAA Journal*, Vol. 20, No. 1, 1982, pp. 33–38.

[7]Baldwin, B. S., and Barth, T. J., "A One-Equation Turbulence Transport Model for High Reynolds Number Wall-Bounded Flows," NASA TM 102847, Aug. 1990.

[8]Kandula, M., and Buning, P. G., "Evaluation of Baldwin-Barth Turbulence Model with Thin-Layer Navier-Stokes Computation of an Axisymmetric Afterbody-Exhaust Jet Flowfield," AIAA Paper 93-0418, Jan. 1993.

[9]Buning, P. G., Chen, W.M., Renze, K. J., Sondak, D., and Chiu, I. T., "OVERFLOW / F3D User's Manual, Version 1.6n," NASA Ames Research Center, Moffett Field, CA, Oct. 1991.

Parallelization of the Factored Implicit Finite Difference Technique

Abraham N. Varghese*
Naval Undersea Warfare Center,
Newport, Rhode Island 02841
and
Peter E. Raad†
Southern Methodist University, Dallas, Texas 75275

Introduction

PHYSICAL phenomena governed by differential equations give rise to systems of coupled algebraic equations, requiring the solution of matrices. The coefficient matrices that result from finite difference implementations in fluid dynamics are banded. In the last two decades, several solution techniques have been developed to take advantage of the diagonal nature of the resulting system of equations. All were developed though in the context of a serial computer, seeking to minimize the total work needed for a complete solution while maintaining a high level of accuracy and stability. This paper summarizes a research effort in the parallelization of the Beam and Warming factored implicit technique.[1] The parabolic heat equation and the nonlinear equations of curvilinear grid mapping were chosen as model equations. Additional information may be found in Varghese.[2]

Parallel Implementations and Results

The factored implicit (FI) technique was implemented in Fortran on the Sequent 20-processor Symmetry computer which has a tightly coupled multiple instruction stream–multiple data stream (MIMD), shared memory, multiprocessor architecture. Speedup calculations were made based on the definition of the speedup S being equal to the ratio of the most efficient serial algorithm time to the parallel algorithm time with P processors running. Parallel compilers such as the Sequent's provide parallelization directives such as *C$DOACROSS* (hereafter referred to in shorthand as *C$DO*), which automatically handles do loops, and *M_FORK* (hereafter referred to as *M_F*) which provides the programmer with selective con-

Received March 2, 1992; revision received Feb. 4, 1993; accepted for publication March 10, 1993.

*Mechanical Engineer, Code 8232, Building #108.
†J. Lindsay Embrey Trustee Associate Professor, Department of Mechanical Engineering.